Supporting Information

Enhancing Aluminum Foil Performance in Aqueous and Organic Electrolytes: Dual-Secure Passivation with Phthalocyanine as a Corrosion Inhibitor

Teshager Mekonnen Tekaligne[a], Hailemariam Kassa Bezabh[a], Semaw Kebede Merso[a], Kassie Nigus Shitaw[a], Misganaw Adigo Weret[a], Yosef Nikodimos[a], Shi-Kai Jiang[a], Sheng-Chiang Yang[a], Chia-Hsin Wang[d], She-Huang Wu[b, c], Wei-Nien Su[* b, c], Bing Joe Hwang[*a, c, d]

[a]Nano-electrochemistry Laboratory, Department of Chemical Engineering, National Taiwan University of Science and Technology, Taipei City 106, Taiwan.

[b]Nano-electrochemistry Laboratory, Graduate Institute of Applied Science and Technology, National Taiwan University of Science and Technology, Taipei City 106, Taiwan

[c]Sustainable Electrochemical Energy Development Center, National Taiwan University of Science and Technology, Taipei City 106, Taiwan.

[d]National Synchrotron Radiation Research Center (NSRRC), Hsinchu 30076, Taiwan

Corresponding authors:

Bing Joe Hwang (bjh@mail.ntust.edu.tw)

Wei-Nien Su (wsu@mail.ntust.edu.tw)

1. Experimental section

1.1. Material preparation

Phthalocyanine (Pc) was all supplied by Thermo Fisher Scientific, USA. Lithium bis(trifluoromethanesulfonyl)imide (LiTFSI), zinc trifluoromethyl sulfonate ($Zn(OTf)_2$), aluminum foil (0.1 mm thickness), and zinc foil (0.02 mm thickness) were purchased from Sigma Aldrich. LiTFSI and $Zn(Otf)_2$ salts were dissolved in deionized water in the calculated amounts to make the electrolyte. The Pc additive amount was optimized using concentrations of 0.5, 1, and 2 wt%. To make the electrolyte, LiTFSI, and $Zn(Otf)_2$ salts were dissolved in deionized water in the calculated amounts.

1.2. Electrochemical measurements

1.2.1. Corrosion measurements

A potentiostat (PGSTAT302N, Metrohm Autolab) built through a rotational system was used to measure the electrochemical activity (Pine Research Instrumentation, Durham, NC, USA). The measurements were conducted employing a three-electrode configuration through a reversible hydrogen electrode serving as the reference electrode, graphite serving as the counter electrode, and aluminum as the working electrode for corrosion studies. The electrode was initially soaked in the sample solution before the testing to establish a consistent corrosion potential. Measurements of Potentiodynamic polarization have been conducted using a 21m LiTFSI electrolyte with and without 1 wt% Pc additives.

1.2.2. Cell performance test

In all electrochemical measurements, a coin cell of the CR2032 type was employed for the battery charge/discharge test. The zinc foil (16 mm diameter disc) served as the anode, and the LVPF (13 mm diameter disc) was the cathode. The charge/discharge tests were performed at room temperature using an Arbin Instruments BT-2000 40-channel battery tester and a 400 µm thick glass fiber as the separator. Li-salt and Zn-salt electrolyte was composed of 21 m LiTFSI and 2 m $Zn(Otf)_2$, and 1 wt% Pc was added as a corrosion inhibitor for aluminum. The Zn||LVPF full cell used to have a potential window between 0.6 and 2.2 V during charging and discharging. The electrochemical performance of an Al/LVPF/21m LiTFSI+2m $Zn(Otf)_2$/Zn dual ion battery and self-discharge was investigated at a rate of 0.2 C with and without additive. Cyclic voltammetry investigation for the Zn||LVPF cell was conducted using a potentiostat (BioLogic VMP3) and a 0.6 V to 2.2 V potential window with 0.2 mV s^{-1} scan rate.

1.3. Surface characterization

Al current collector was collected by rinsing it in water and letting it dry under a vacuum before examining the sample's surface. This was done after completing Potentiodynamic polarization measurements on the sample. To analyze the morphology of aluminum surface samples in the presence and absence of Pc, we used the SEM-EDS method with a product code of FE-SEM, JSM-6500F, JEOL, and a magnification of 1000 µm of the surfaces of the Al metal. The gold

Au 4f-800 peak at 84 eV is employed as the reference point for the binding energy scale in all X-ray photoelectron spectroscopy (XPS) investigations.

The surface roughness of the samples treated in the aqueous electrolytes with and without Pc additives was examined using an AFM (NX10, AFM Park systems, Suwon, South Korea). Investigations employing XPS were carried out in Hsinchu, Taiwan, at the National Synchrotron Radiation Research Center (NSRRC24A1) and TPS-44A beamlines while maintaining a 25 °C air temperature. On a PerkinElmer Spectrum Two system (PerkinElmer, Buckinghamshire, U.K.), infrared spectra (FT-IR) were collected throughout a wavenumber range of 4000–600 cm^{-1}. Utilizing corrosion byproducts produced on the aluminum surface during polarization, FT-IR spectra were taken. A 10 mm quartz cuvette and the PerkinElmer Lambda 1050 were used to perform ultraviolet-visible (UV-vis) spectroscopy to confirm the formation of insoluble AlPc-F thin film on the Al surface.

2. Computational Details

Recently, computational techniques have been used to simulate the molecular characteristics of organic, inorganic, and condensed material[1-6]. Researchers have associated these molecular characteristics with the capacity of these molecules to suppress corrosion[7-9]. Applying the Gaussian 09 software, Density functional theory calculations were performed to optimize all geometrical structures for isolated PCs operating at room temperature[10-12]. Lee-Yang-Parr (LYP) gradient-corrected correlational functional and Becke's (B3) three-parameter hybrids

function are integrated into the hybrid parameter B3LYP/6-311G (d, p) approximation[13-18] was used with the basic set of 6-311G following the set of d, p polarization functions to obtain the data presented in this study[18]. Due to computational cost and accuracy, several studies have investigated the above for theoretical ALIBs studies[16-18].

2.2. DFT Calculations

Density Functional Theory (DFT), which models a system's ground state electronic properties as a function of its electron density, is one of these computational techniques. These computational techniques have several advantages over experimental ones, one of which is the absence of statistical error, which experimental data collection and analysis are susceptible to[8]. According to research, a molecule's capability to suppress corrosion is influenced by its electronic properties, which can be inferred from quantum chemical parameters such energy gap the energy gap(ΔE) between the LUMO and HOMO[3, 19, 20].

The relationship between such a metal's ionization potential (I), which is correlated with the energy of its highest occupied molecular orbital (E_{HOMO}), and an inhibitor's potential to donate electrons into low-lying empty orbitals, is given by the following formula:

$$I = \quad - E_{HOMO} \tag{1}$$

Furthermore, the electron affinity (A) of an inhibitor correlate to the energy of the lowest unoccupied molecular orbital or E_{LUMO}, and it denotes the inhibitor's tendency to accept

electrons.

$$A = -E_{LUMO} \quad (2)$$

The energy gap (E) of inhibitors decreases due to a subsequent increase in their reactivity, which increases the anticipated corrosion inhibition potential.

Table S1: Quantum chemical parameters of the related works for the Pc additive that were calculated

Additives	$E_{HOMO}\,(eV)$	E_{LUMO} (eV)	ΔE_{gap} (eV)	μ (Debye)	IE (eV)	AE (eV)
Q1[21]	−4.807	−0.695	4.172	3.085	4.807	0.695
Q2[21]	−5.065	-1.286	3.778	2.666	5.065	1.286
PSC-A[22]	−5.690	-0.600	5.090	N.A	5.690	0.600

Where: Q1 = ethyl 2-(4-(2-ethoxy-2-oxoethyl)-2-p-tolylquinoxalin-1(4H)-yl)acetate
Q2 = 1-[4-acetyl-2-(4-chlorophenyl)quinoxaline-1(4*H*)-yl]acetone
PSC-A = (E)-2-(1-(2-hydroxyethylamino) ethylimino)ethyl phenol
N. A= not available.

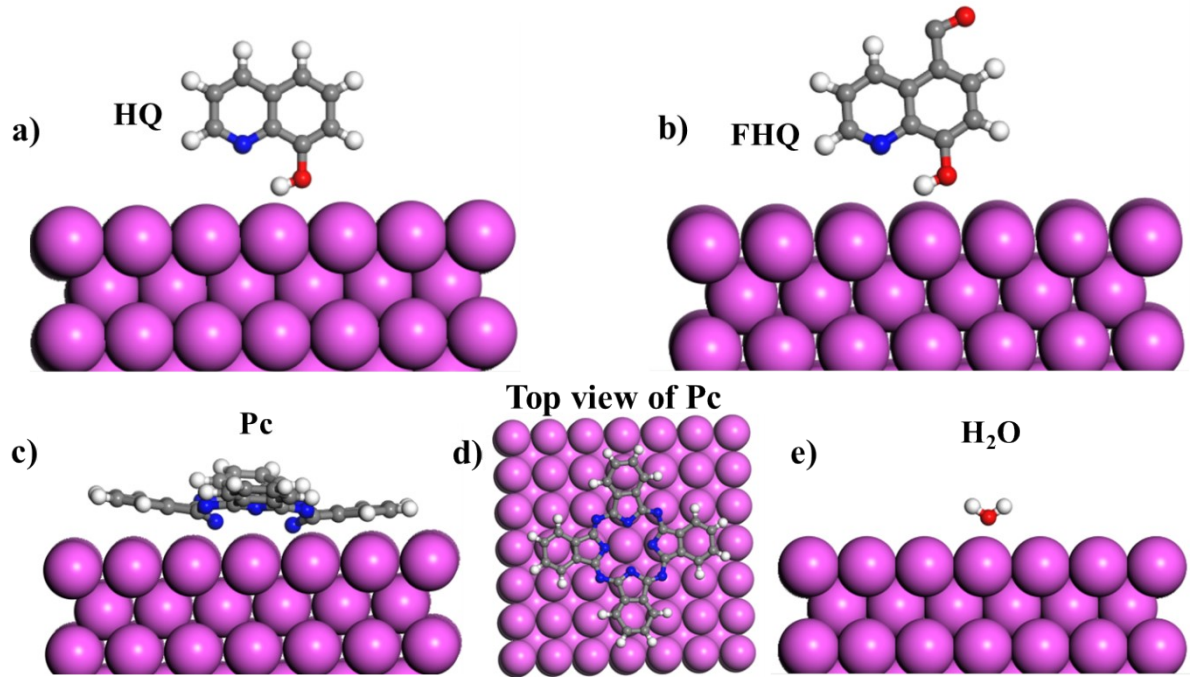

Fig. S1 DFT calculation on the adsorption energy of a) HQ b) FHQ, c) Pc, and d) Top view of Pc, and e) H_2O molecules on the Al surfaces.

3. **Experimental Section**

The surface morphology of aluminum samples was studied using the SEM method after Potentiodynamic polarization measurements (model: FE-SEM, JSM-6500F, JEOL) and for the surfaces of the Al current collector. Potentiodynamic polarization measurement conducted by bare Al foil is used as a current collector, which act as a working electrode for the electrolyte with and without Pc additive. The gold Au 4f-800 peak at 84 eV was used as the calibration point for the binding energy scale for all X-ray photoelectron spectroscopy (XPS) research. The 24A1 and TPS-44A beamline stations of the National Synchrotron Radiation Research Center (NSRRC) in Hsinchu, Taiwan, were used for XPS investigations. Utilizing the corrosion byproducts created on the metal surface during polarization, FT-IR spectra were taken. The possibility of inhibitor adsorption on metal surfaces is demonstrated in this investigation.

The electrochemical activity was assessed using a potentiostat (PGSTAT302N, Metrohm Autolab) with a rotational mechanism (Pine Research Instrumentation, Durham, NC, USA). 21m LiTFSI, with 1 wt% Pc electrolytes were used for Potentiodynamic polarization measurements.

The calculated values are listed in **Table S2** for LiTFSI with/without additives from

Potentiodynamic polarization measurement.

Table S2. Polarization parameters of the electrolyte samples with and without additive

Sample	I_{corr} (μA)	E_{corr} (mV)	Corrosion rate (CR, mmpy)	η
21 m LiTFSI w/o Additive	0.302	360.597	9.881 x10^{-3}	-
21 m LiTFSI+1 wt% Pc	0.013	513.285	4.26 x10^{-4}	23.23
21 m LiTFSI+1 wt% HQ[23]	0.112	417.548	3.66 × 10^{-3}	2.696
21 m LiTFSI+1 wt% FHQ[23]	0.042	509.856	1.37 × 10^{-3}	7.190

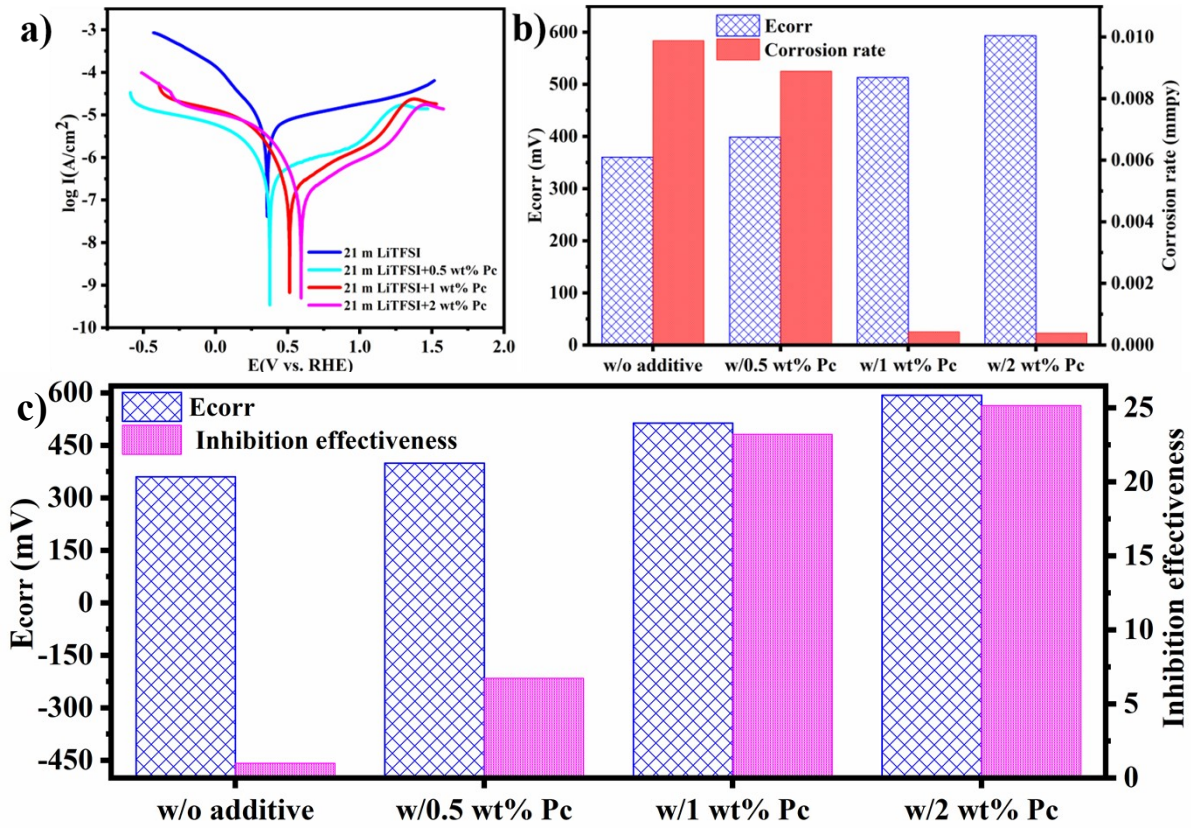

Fig. S2 a) Potentiodynamic polarization curves for 21 m LiTFSI and with 0.5, 1, and 2 wt% Pc, b) Relationship between Corrosion potential and corrosion rate, c) c) corrosion potential vs. inhibition effectiveness with different concentration of Pc additive.

Table S3. Electrochemical parameters of aluminum in the absence and presence of different amounts of Pc additive

Electrolytes with/without additives	E_{corr} (mV)	I_{corr} (μA cm^{-2})	βa (mV dec^{-1})	βc (mV dec^{-1})	CR (mmpy)	η
1m LiTFSI w/o Pc	-354.887	0.703	689.4	261.6	0.022	-
1 m LiTFSI+1 wt% Pc	-387.120	0.385	533.2	393.4	0.013	1.83
21 m LiTFSI w/o Pc	360.597	0.302	114.5	123.1	0.0098	-
21 m LiTFSI+0.5 wt% Pc	399.119	0.272	365	177.7	0.0089	6.73
21 m LiTFSI+1 wt% Pc	513.285	0.013	116.7	117.5	0.00042	23.23
21 m LiTFSI+2 wt% Pc	593.335	0.012	121.7	117.5	0.00039	25.17

$$CR = \frac{I_{corr} \times k \times EW}{\rho \times A} \times 100 \quad (3)$$

Where CR is corrosion rate, Icorr is corrosion current density, EW is equivalent weight, ρ is density, A is the area of the electrode used as the current collector.

The following equations from the corrosion potential can be used to derive the corrosion current density since the corrosion potential (Ecorr) is the driving force (Ecorr-Eeq)[24, 25].

$$Icorr = \frac{Ecorr - Eeq}{R} \quad (4)$$

Where Icorr, Ecorr, Eeq, and R are corrosion currunt density, corrosion potential, the equilibrium potential corrosion reactions, and resistance, respectively

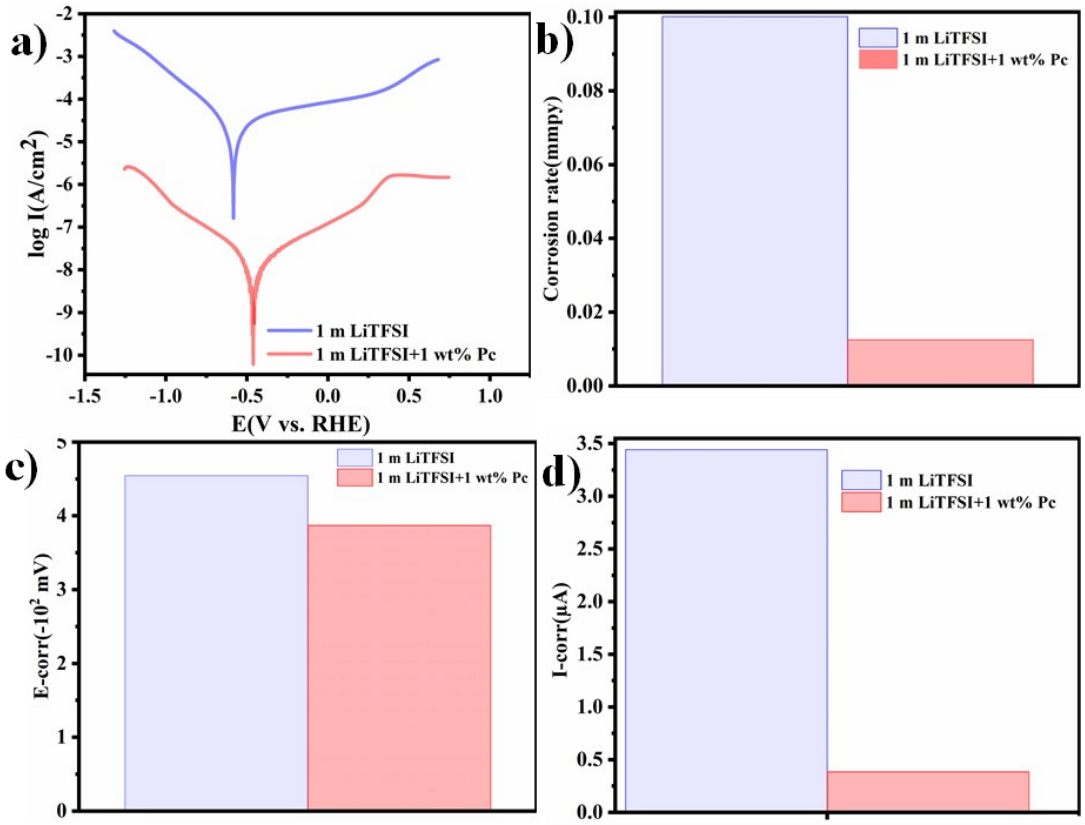

Fig. S3 a) Potentiodynamic polarization curves for 1 m LiTFSI and with 1 wt% Pc; Tafel fit results after Potentiodynamic polarization measurements for 1 m LiTFSI and with 1 wt% Pc, (b) corrosion rates; (c) Corrosion potential E_{corr}; (d) Corrosion current density $I_{corr.}$

The addition of Pc, as seen in **Fig. S3** and Table S2, caused the E_{corr} to reach a higher positive value.

a)

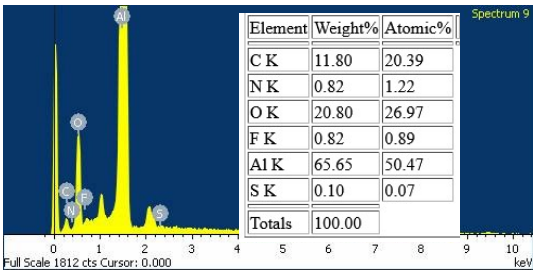

Element	Weight%	Atomic%
C K	11.80	20.39
N K	0.82	1.22
O K	20.80	26.97
F K	0.82	0.89
Al K	65.65	50.47
S K	0.10	0.07
Totals	100.00	

b)

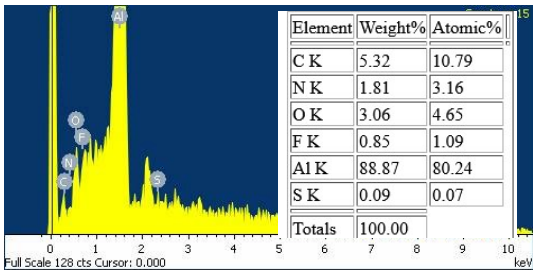

Element	Weight%	Atomic%
C K	5.32	10.79
N K	1.81	3.16
O K	3.06	4.65
F K	0.85	1.09
Al K	88.87	80.24
S K	0.09	0.07
Totals	100.00	

Fig. S4 EDS results of the Al surface after linear polarization for a) w/o additive, b) w/Pc.

Table S4. The viscosity of electrolyte solution at different concentrations measured at 25 ºC

Electrolyte	Average run-time(s)	Density (g/cm^3)	Viscosity (mP.s)
Standard solution	10.720	0.997	0.890
21 m LiTFSI+2 m $Zn(OTf)_2$	47.059	1.976	2.533
21 m LiTFSI+2 m $Zn(OTf)_2$+0.5 wt% Pc	63.795	2.049	3.321
21 m LiTFSI+2 m $Zn(OTf)_2$+ 1 wt% Pc	68.296	2.326	3.985
21 m LiTFSI+2 m $Zn(OTf)_2$+2 wt% Pc	83.256	2.462	5.151

Surface analysis from chemical tests

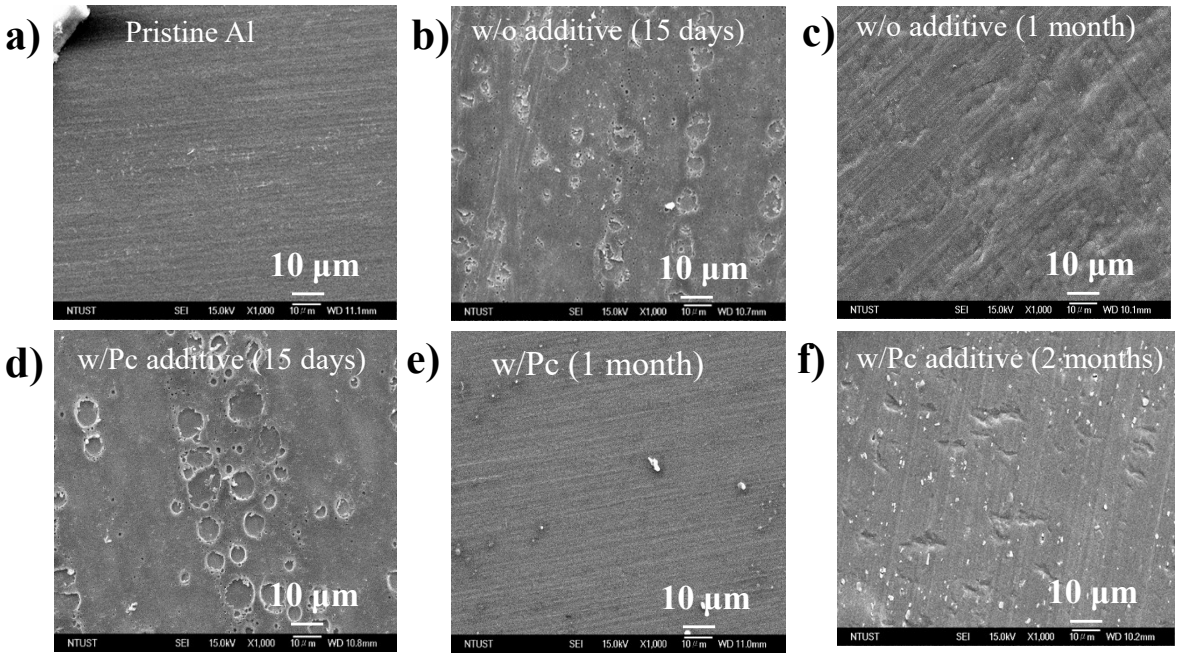

Fig. S5 SEM images for chemical tests, a) Pristine Al, b) w/o additive (15 days), c) w/o additive (1 month), d), w/Pc additive (15 days) e), w/Pc (1 month) and f), w/Pc additive (2 months).

Electrochemical impedance Spectra

The imaginary component(Z") is plotted with the real component (Z′) of the impedance. The Al foil resistance to corrosion values for the electrolyte containing the Phthalocyanine additive (**Fig. S6b**) was significantly higher when compared to the electrolyte without additive substrate (**Fig. S6a**).

The constant phase element or CPE was used to explain the non-ideal behavior of the capacitance characteristics of the metal surface as it relates to the heterogeneity of the interface. Surface roughness, inhibitor molecule adsorption, and surface layer deposition on the metals are the sources of surface heterogeneity[26]. This is related to the reality that the surface of such samples exhibits non-ideal behavior as a result of the surface's heterogeneity[27, 28]

From the impedance spectra (**Fig. S6**), the diameter of the arcs can be utilized to estimate the electrochemical impedance[29]. Generally, the diameter of the semicircle is often positively associated with the anti-corrosion of the specimen. The larger the diameter of the semicircle, the better the corrosion resistance[30].

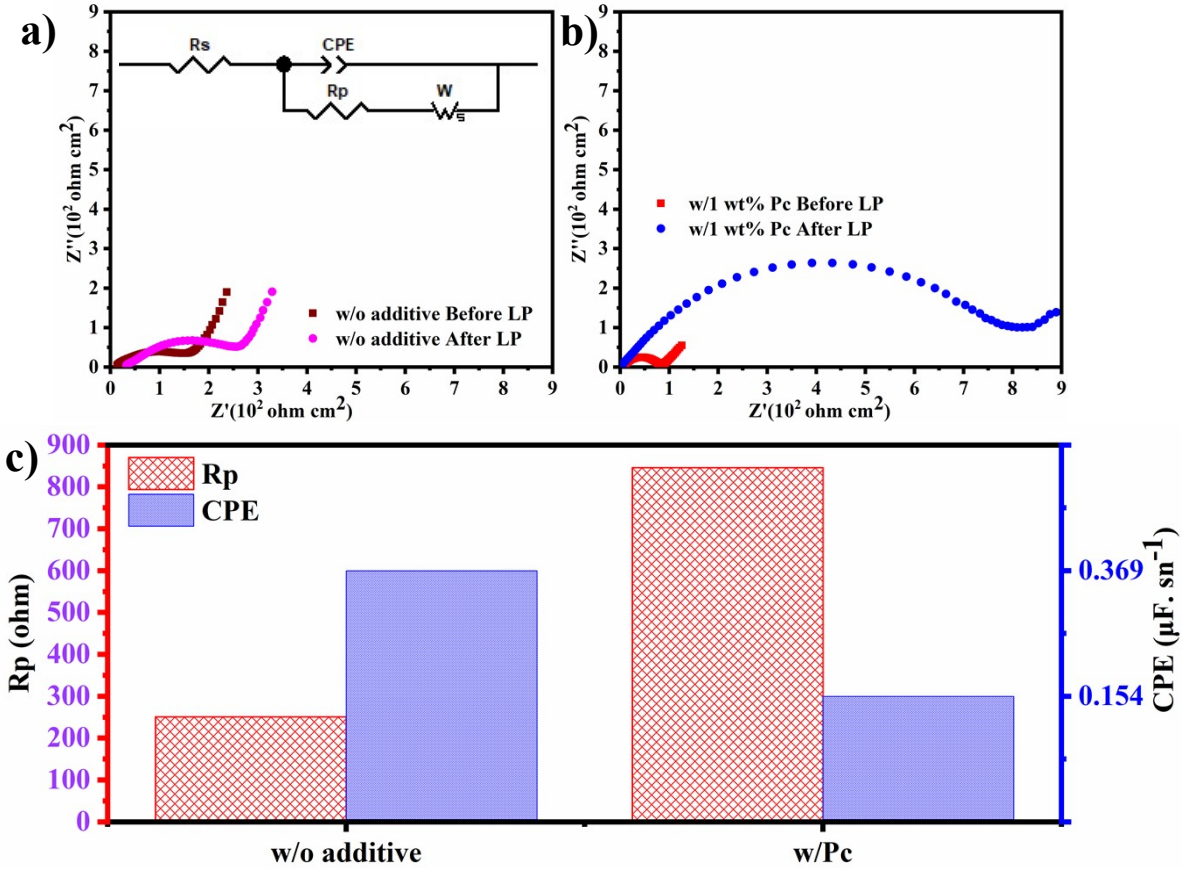

Fig. S6 Electrochemical impedance spectra before and after Potentiodynamic polarization measurements, (a) 21 m LiTFSI without additives, the inset is equivalent circuit fit, (b) with 1 wt% Pc, and (c) polarization resistance and CPE with and without additives.

The equivalent circuit with constant phase element (CPE) rather than the pure capacitor was used due to the surface reaction, electrode porosity, surface roughness, and heterogeneity in the studied system[31] as shown in **Fig. S6c**. After linear polarization measurements, the Pc additive in an aqueous electrolyte for an Al foil current collector showed the highest total resistance. As was said at the beginning of this section, the development of an AlPc-F film on the aluminum surface generates a barrier effect that protects against corrosive substances. The increasing trend in resistance values associated with Pc additive can be recognized as the

inhibitive Pc layer formation on the Al surface.

Table S5. Impedance parameters for corrosion off Al current collector in 21 m LiTFSI with and without additives at 298 K after LP.

Electrolytes	R_s(ohm)	R_p(ohm)	CPE (F. s^{n-1})
w/o additive	1.951	251	3.690×10^{-7}
w/1 wt% Pc	11.837	825	1.540×10^{-7}

Note: Rs=Solution resistance, Rp=polarization resistance, CPE=Constant Phase Element

Table S6. Average roughness of aluminum surface obtained by AFM after Potentiodynamic treatment with and without additives.

Sample	**S_a (average roughness)**
Bare Al	19.50 nm ±0.060
w/o additive	1.57 µm ±0.050
With 1 wt% Pc	0.111 µm ±0.009

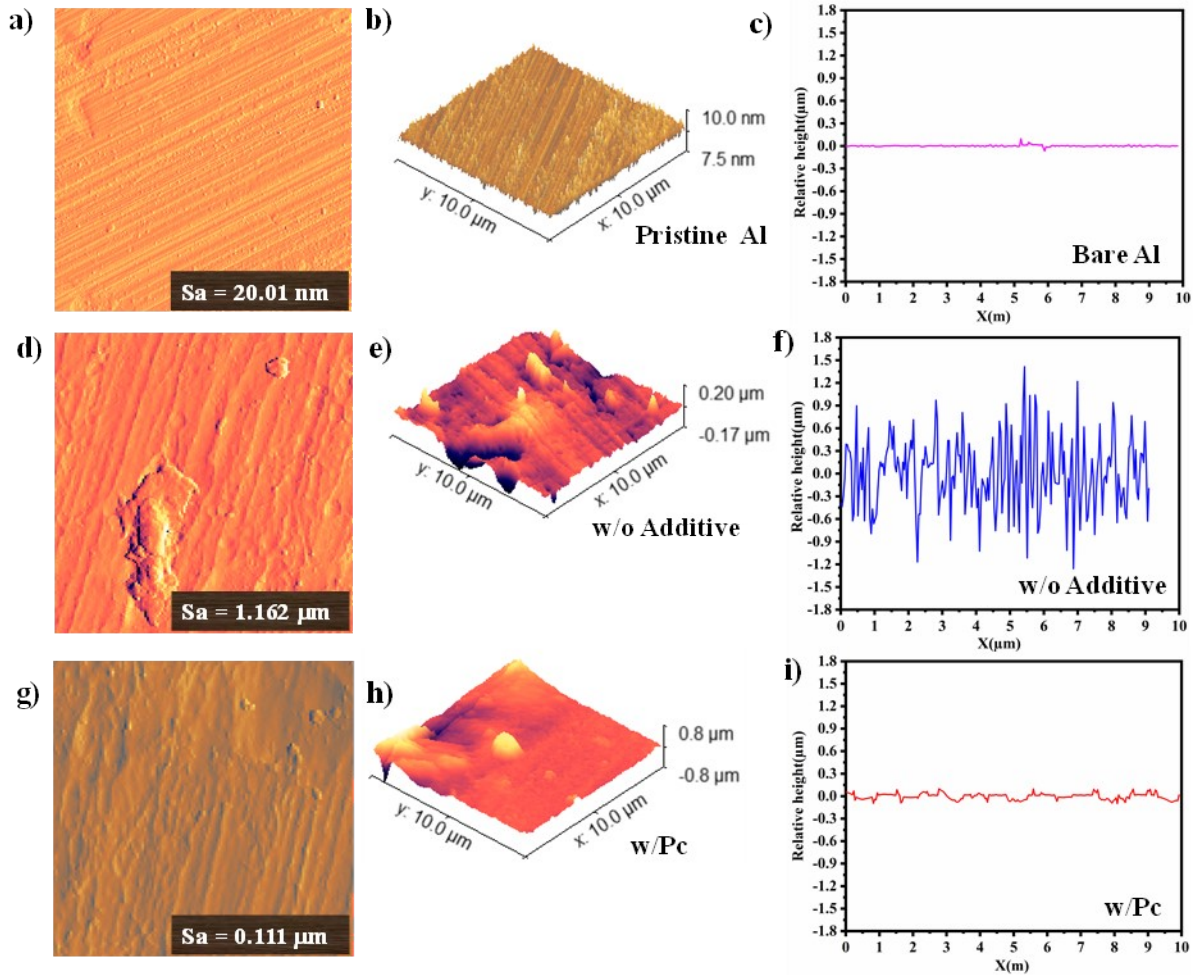

Fig. S7 Average roughness of aluminum surface after Potentiodynamic polarization or anodizing treatment in (a), (b), and (c) for Pristine Al (d), (e), and (f) are for electrolyte w/o additive and (g), (h) and (i) are for electrolyte w/Pc additive obtained by AFM.

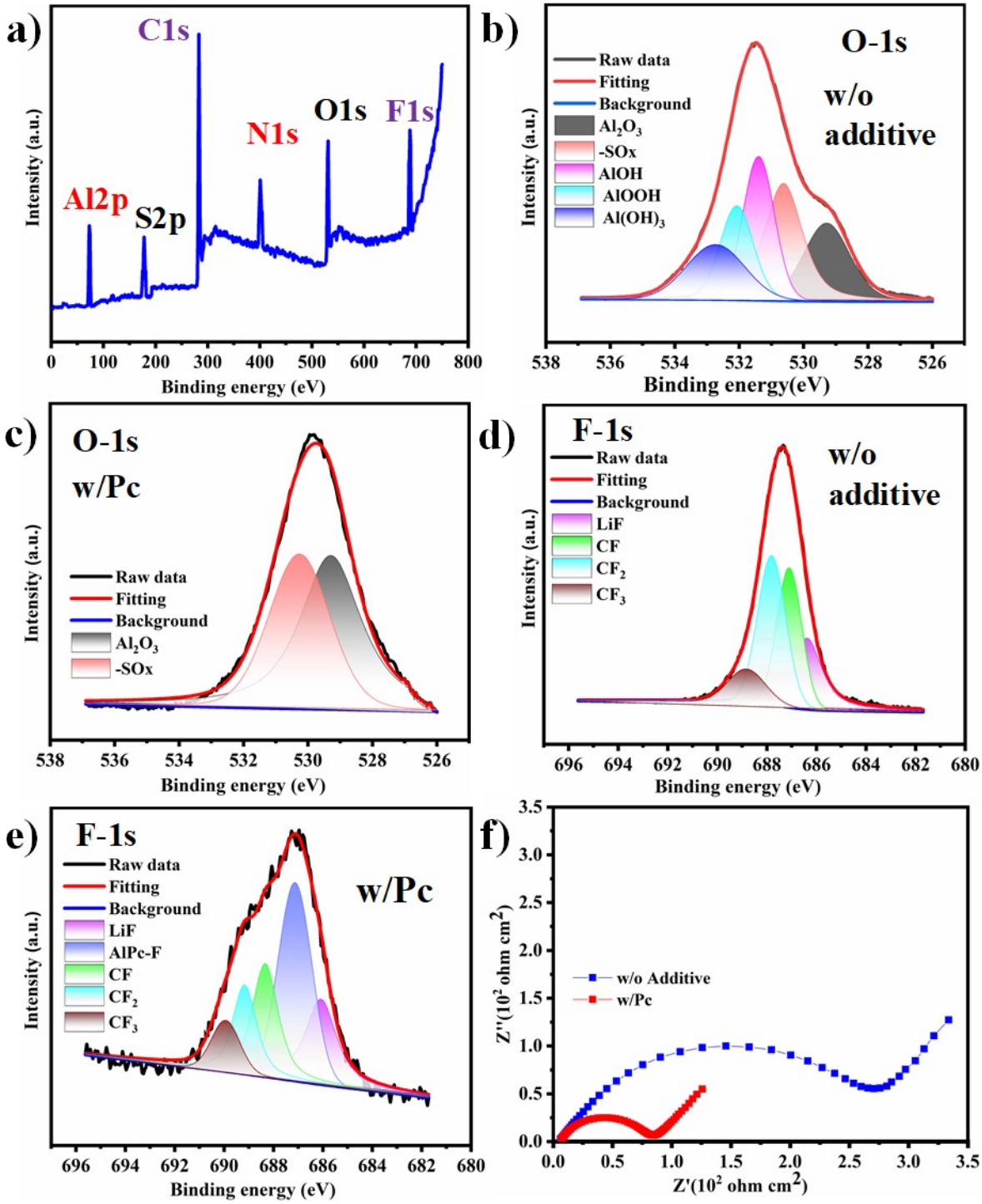

Fig. S8 X-ray photoelectron spectrum for (a) XPS spectrum survey for the sample after Potentiodynamic polarization, (b) O 1s for pristine; (c) O 1s for the electrolyte w/Pc additive; (d) F 1s for pristine, (e) F 1s for the electrolyte w/Pc additive, (f) EIS for the electrolyte with and without additive.

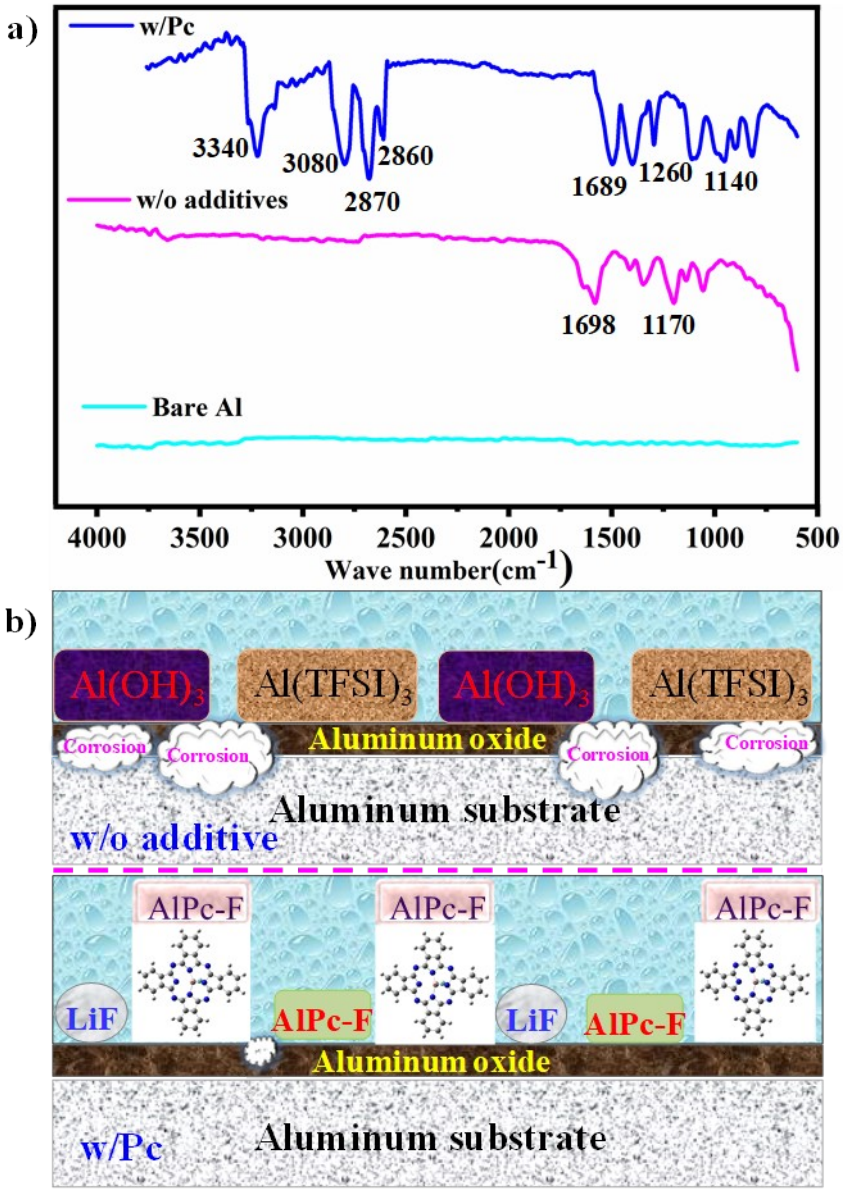

Fig. S9 a) FT-IR spectroscopy analysis of Al surface, b) The moieties involved in the passivation layer of an aluminum current collector.

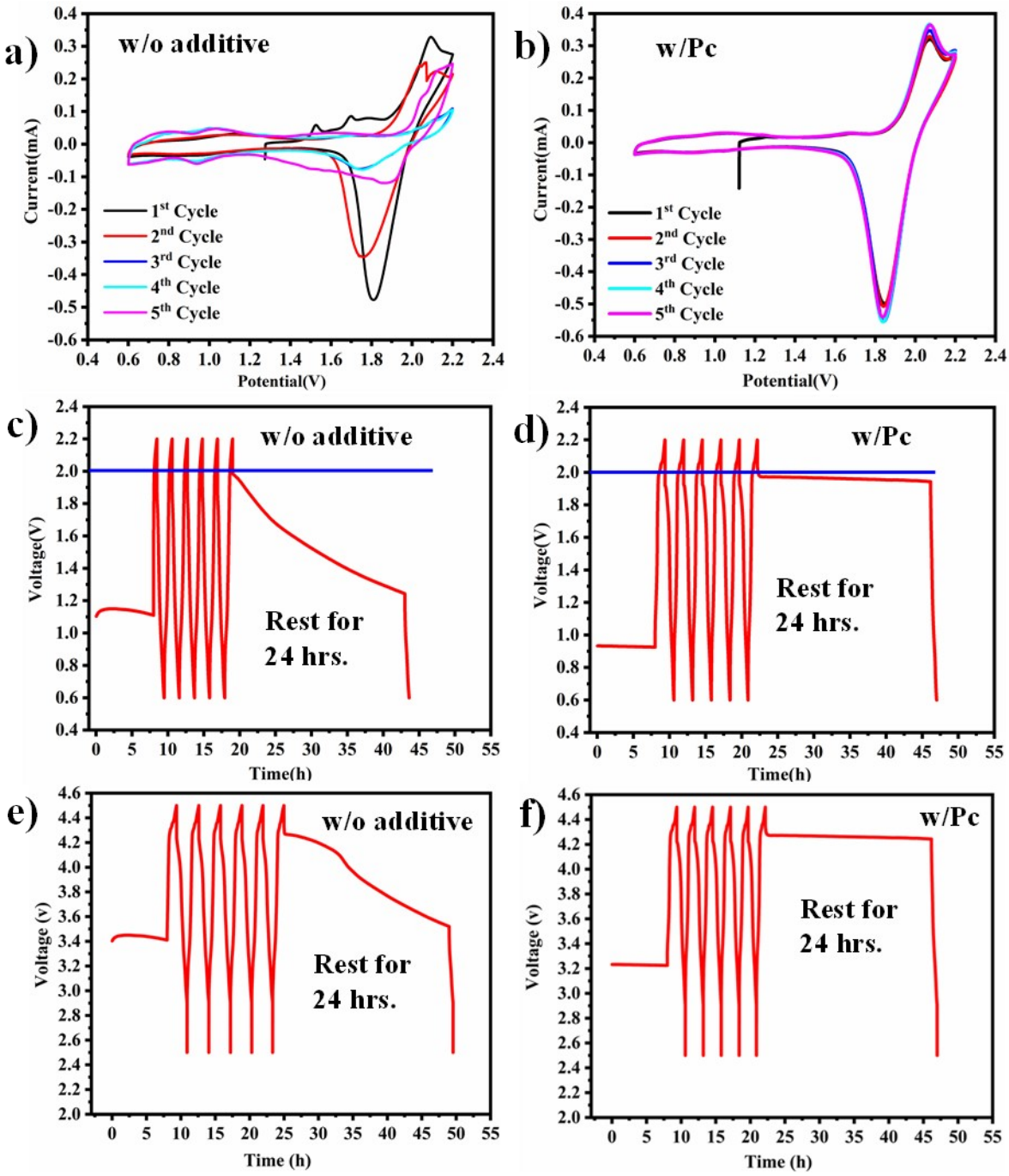

Fig. S10 Cyclic voltammetry curves for LVPF cathodes with Al foils as current collectors through 21m LiTFSI+2 m $Zn(OTf)_2$ aqueous electrolytes with and without additives at 0.2 C-rate for (a) w/o additive, (b) w/Pc, Self-discharge tests for (c) w/o additive, and (d) w/Pc, self-discharge test of the three-electrode system, LVPF as working electrode coated on Al current collector, Li metal as both counter and reference electrode, e) w/o additive, f) w/Pc.

The ionic conductivities of electrolyte solutions were examined and measured utilizing symmetric stainless steel through impedance spectroscopy tests. To calculate bulk resistance (R), the following formula was used:

$$R = \rho \frac{l}{A} \quad (5)$$

Where R is bulk resistance, ρ is resistivity, L is the distance between two electrodes (considered equal to the thickness of the separator used (400 μm thick)), and A is the cross-sectional area of the stainless steel.

The following formula can be used to quantify ionic conductivity (σ):

$$\sigma = \frac{l}{RA} \quad (6)$$

Before cycling, pristine cells produce larger interfacial resistance (from the semicircle arc at a high frequency) than additive ones (Pc), as seen in **Fig. S10**. The additives could be admitted to the passivation surface layers of Al foils.

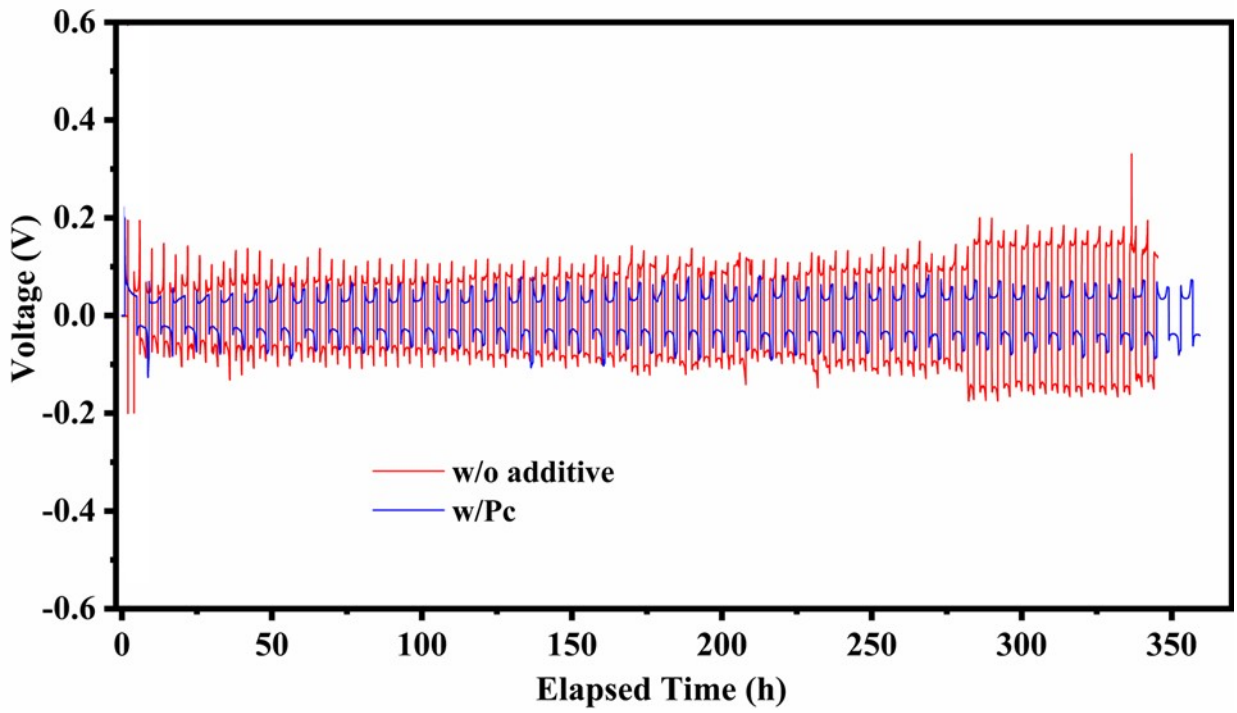

Fig S11. Electrochemical investigation of Zn||Zn symmetric cells prepared with w/o additive (red color) and w/Pc additive (blue color) at 2 mA/cm^2 current density.

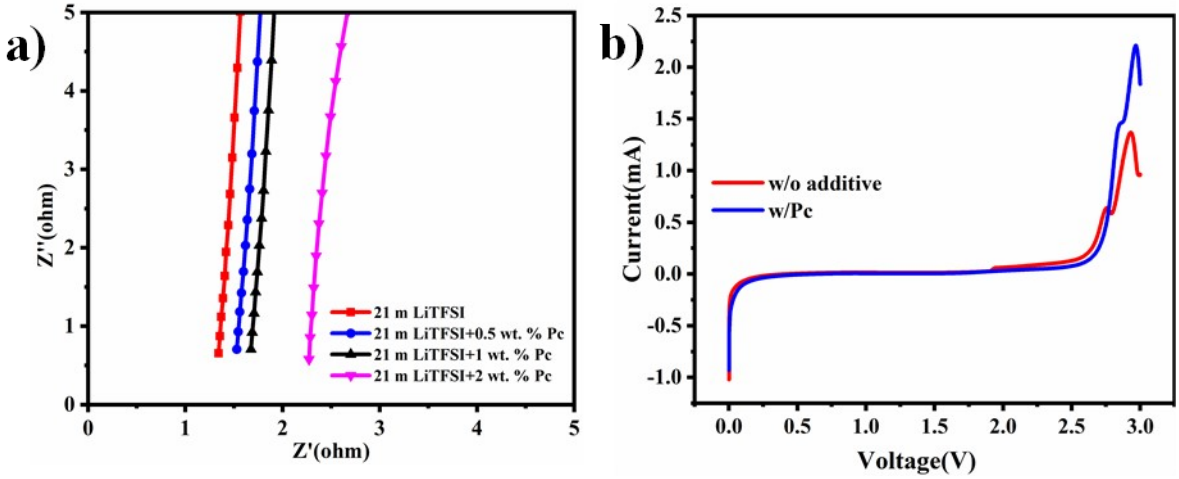

Fig. S12 (a) Impedance spectra of electrolyte with and without 0.5, 1, and 2 wt% Pc additives in the range of 0.01 Hz to 1.00 MHz with an amplitude of ±10 mV using a Biologic Science Instruments coupled with a Frequency Response Analyzer. (b) LSV w/o and w/1 wt% Pc

additive.

Table S7. Summary of the bulk resistances and ionic conductivity of electrolyte obtained from EIS measurement of SS||SS cell at room temperature. The numerical values are obtained from EIS data in **Figure S12**.

Electrolyte	$R_{solution}$ (ohm)	Conductivity (mS/cm)
21 m LiTFSI	1.364	1.450×10^{-2}
21 m LiTFSI+0.5 wt% Pc	1.529	1.307×10^{-2}
21 m LiTFSI+1 wt% Pc	1.674	1.189×10^{-2}
21 m LiTFSI+2 wt% Pc	2.271	8.763×10^{-3}

After testing many electrolyte concentrations based on their solution structure and electrochemical efficiency, the 21 m LiTFSI+2m $Zn(OTf)_2$+1 wt% Pc solution was chosen as the best. The solubility of the salt organic additives decreases as the concentration increases beyond 1 wt% which increases the viscosity of the solution resulting in decreasing the diffusion of ions and affecting the wettability of the LVPF electrode in Zn||LVPF full cell data for the electrolyte with 1 wt% Pc additive.

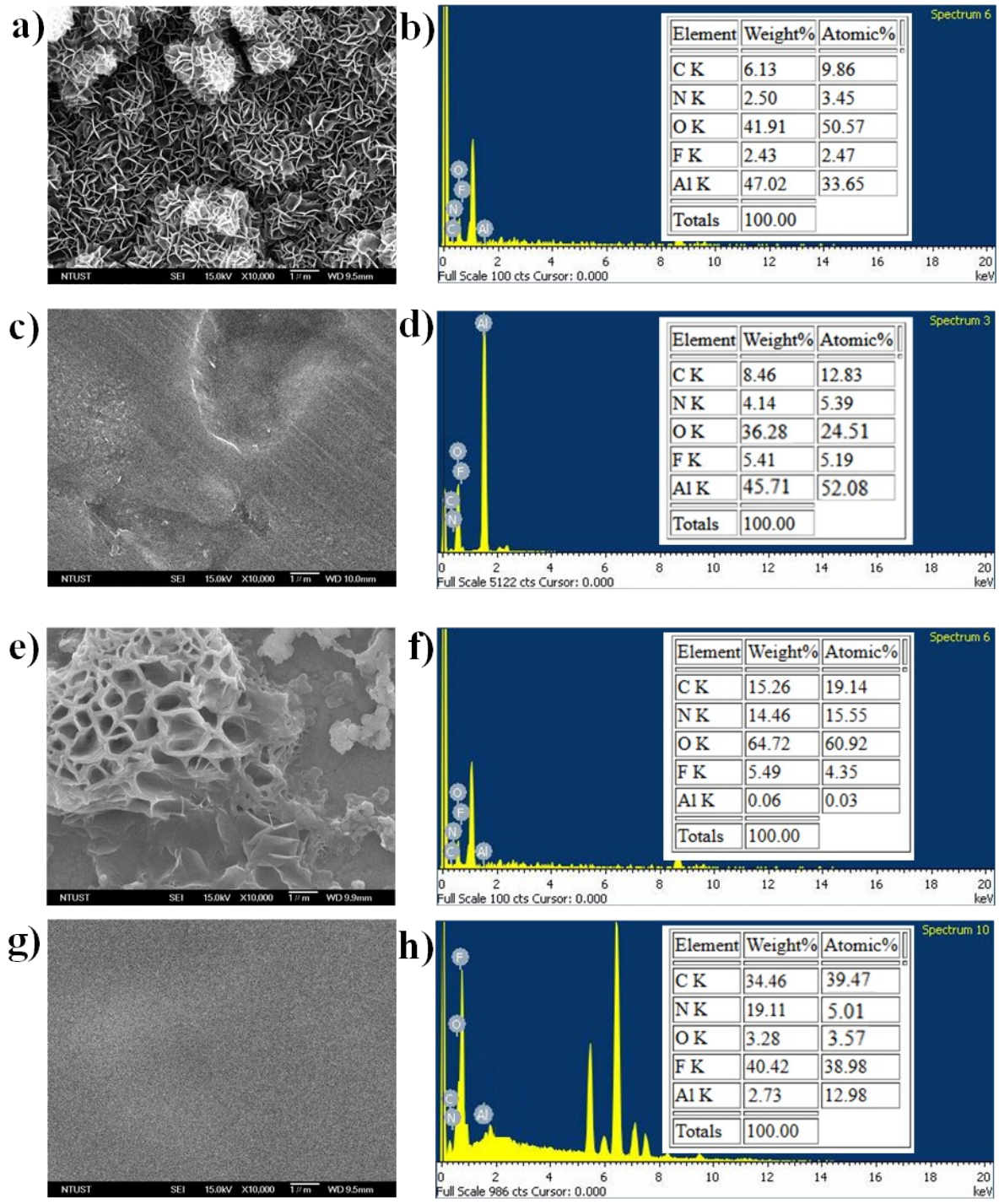

Fig. S13 Morphology and EDS composition of the backside of cycled Al current collector after 5th and 20th cycles. (a) SEM and (b) EDS results w/o additive. after the 5th cycle; (c) SEM and (d) EDS results w/Pc after the 5th cycle; (e) SEM and (f) EDS results w/o additive after the 20th cycle; (g) SEM and (h) EDS results w/Pc after the 20th cycle.

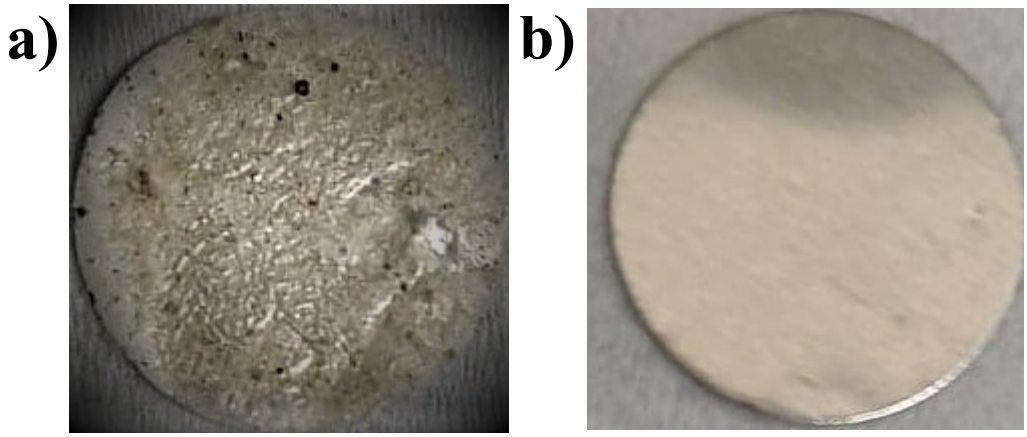

Fig S14. Optical photographs of the zinc foils after the 20th cycling of charge discharge test, a) w/o additive, b) w/Pc additive.

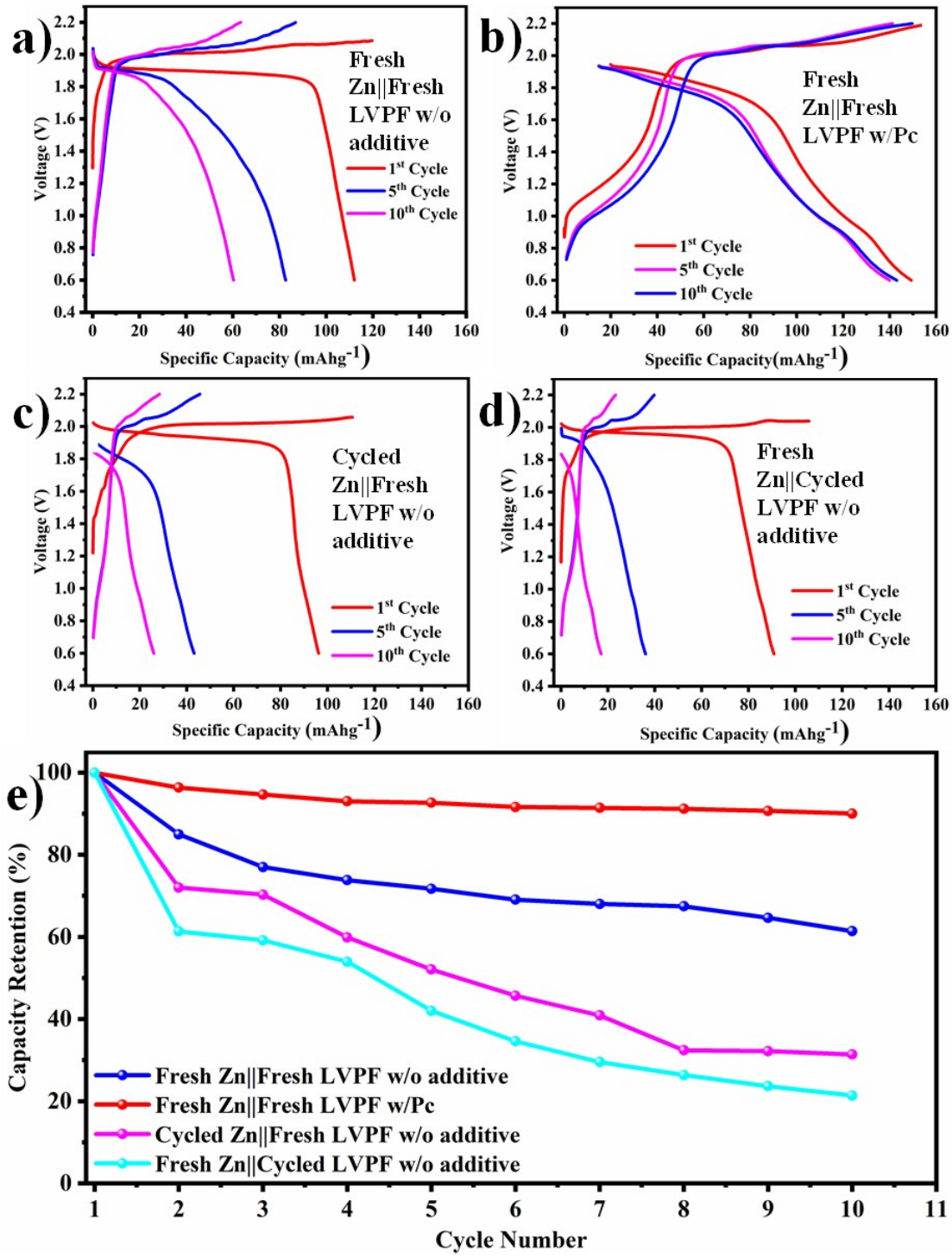

Fig. S15. Zn||LVPF cell to perform capacity fading through cycling for specific capacity of a) Fresh Zn||Fresh LVPF w/o additive, b) Fresh Zn||Fresh LVPF w/Pc, c) Cycled Zn||Fresh LVPF w/o additive, and d) Fresh Zn||Cycled LVPF w/o additive for the electrolyte w/o additive and w/Pc, e) capacity retention vs. cycle number for fresh and cycled electrodes.

Elemental Analysis

The LVPF/Zn coin cells were dissembled after the 10th cycle, and the Zn electrodes, separator, and coin cell components were collected. To extract Al and V from the Zn electrode and separator surface, the Zn electrode and separator were washed with 3 mL acetone for 30 minutes using 10 mL volumetric flasks. Then, the Zn and separator were removed from the flask, and 1 mL HNO_3 (67%) was added to the flasks to digest the samples. After 2 days, the solutions were filtered using a syringe filter (0.2 μm pore size) and diluted to 10 mL using ultra-pure water for the inductively coupled plasma (ICP, 7000 SERIES) test. For the measurement of metal contents on the SS coin cells, the dissembled coin cell components were washed with 6 mL of 1 M HCl for 30 minutes using 10 mL beaker. Then, the solutions were transferred to 10 mL volumetric flask, and about 0.17 mL of HNO_3 was added into the flasks. The resultant solutions were digested for 2 days and then filtered using 0.2 μm pore size syringe followed by diluted to 10 mL for the ICP test. For comparison, 3 mL of pure electrolytes (21 m LiTFSI+2 m $Zn(OTf)_2$ in water with and without Pc additive) were also taken for ICP test. Five standards, containing 2, 4, 6, 8, and 10 ppm of V, Zn, and Al standard solutions, were prepared to calibrate the ICP instrument. Then, the accumulated metallic elements were detected by ICP test (**Fig. S16**). The scanning electron microscopy (SEM, JSM-6500F)-energy dispersive X-ray spectroscopy (EDX) was further used to examine elements on the Al current collector after the 10th cycle full discharge.

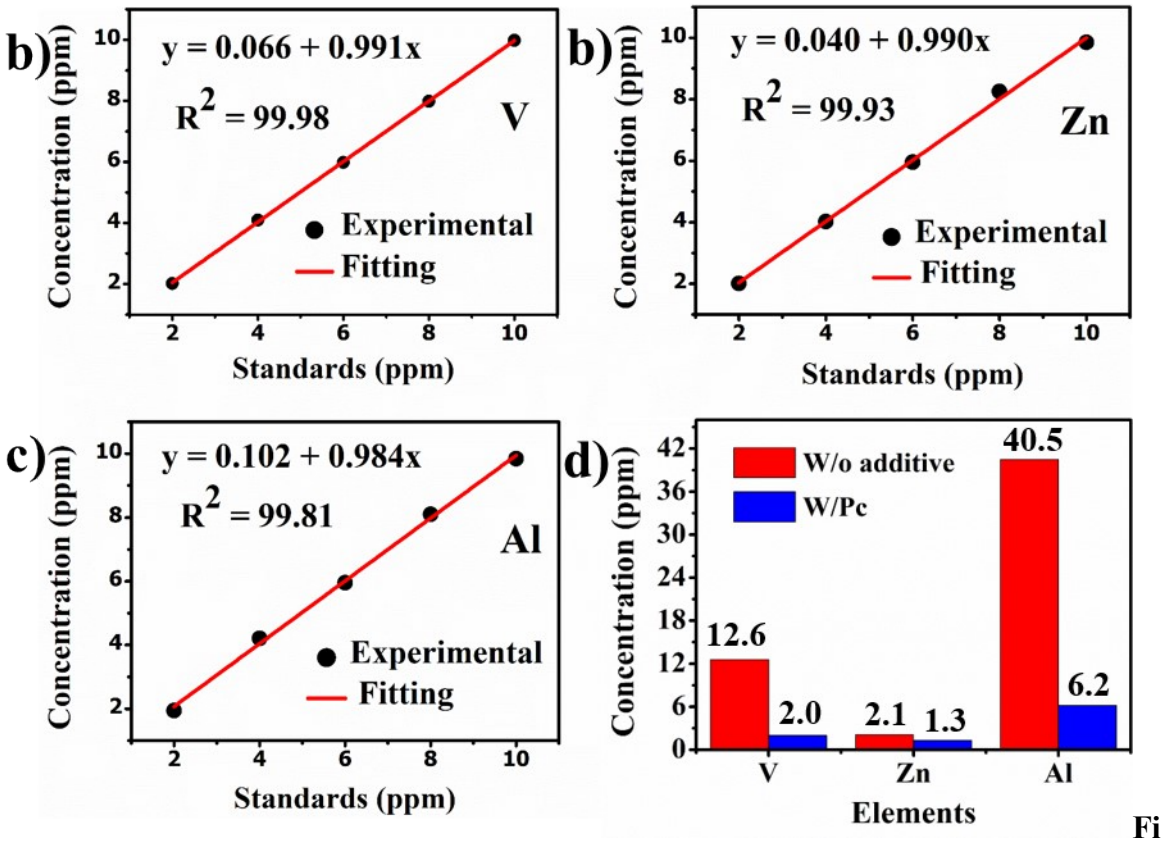

Fig. S16. a-c) ICP calibration fitting d) compression of metallic elements accumulated in the cycled electrolyte after the 10th cycle of LVPF/Zn w/o additive and w/Pc.

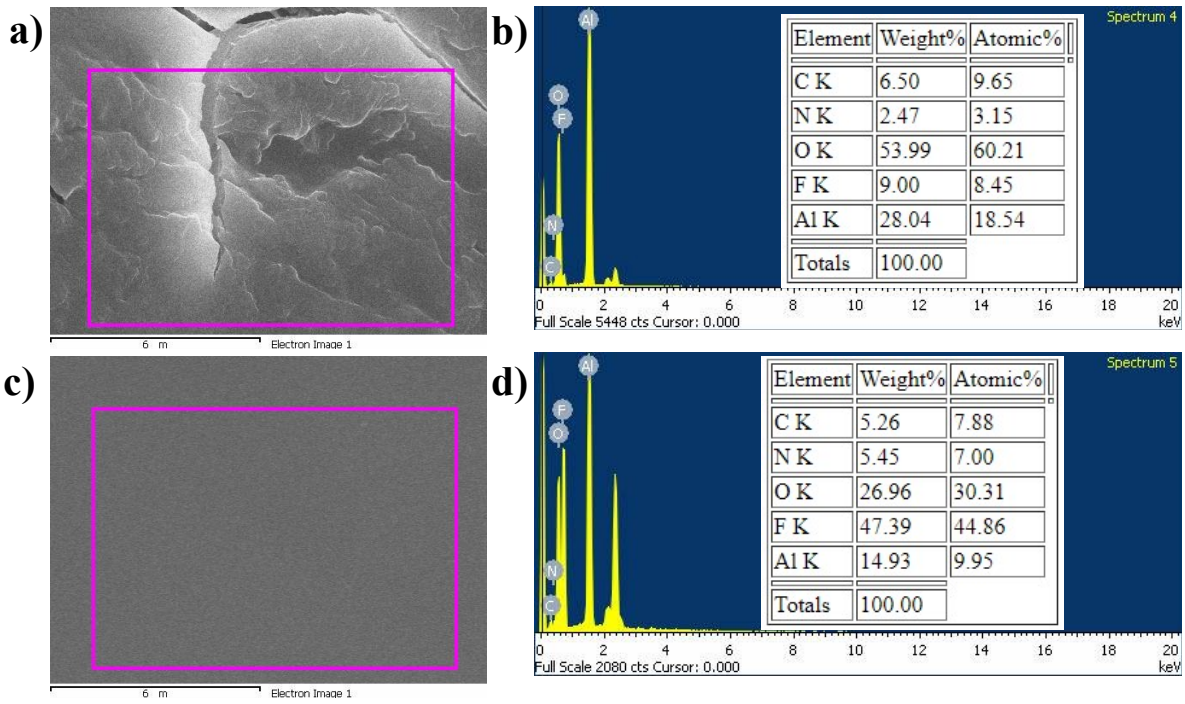

Fig S17. SEM images of an Al current collector by immersion test after 20 days (Chemical test) (a, b) SEM and EDS data for the electrolyte without additive, (c, d) SEM and EDS for the electrolyte with Pc additive.

References

1. I. B. Obot, E. E. Ebenso, N. O. Obi-Egbedi, A. S. Afolabi and Z. M. Gasem, *Research on Chemical Intermediates*, 2012, **38**, 1761-1779.
2. I. Obot, E. Ebenso, I. Akpan, Z. Gasem and A. S. Afolabi, *Int. J. Electrochem. Sci*, 2012, **7**, 1978-1996.
3. I. B. Obot, N. O. Obi-Egbedi, E. E. Ebenso, A. S. Afolabi and E. E Oguzie, *Research on Chemical Intermediates*, 2013, **39**, 1927-1948.
4. I. B. Obot and A. Madhankumar, *Journal of Industrial and Engineering Chemistry*, 2015, **25**, 105-111.
5. A. Döner, R. Solmaz, M. Özcan and G. Kardaş, *Corrosion Science*, 2011, **53**, 2902-2913.
6. N. Obi-Egbedi, K. Essien and I. Obot, *Journal of Computational Methods in Molecular Design*, 2011, **1**, 26-43.
7. I. B. Obot and N. O. Obi-Egbedi, *Current Applied Physics*, 2011, **11**, 382-392.
8. G. Gece, *Corrosion Science*, 2008, **50**, 2981-2992.
9. I. Obot, Z. Gasem and S. Umoren, *Int. J. Electrochem. Sci*, 2014, **9**, 510-522.
10. M. J. Frisch, G. Trucks, H. B. Schlegel, G. Scuseria, M. Robb, J. Cheeseman, G. Scalmani, V. Barone, B. Mennucci and G. Petersson, *Gaussian Inc. Wallingford CT*, 2009, **27**, 34.

11. M. Frisch, G. W. Trucks, H. B. Schlegel, G. E. Scuseria, M. A. Robb, J. R. Cheeseman, G. Scalmani, V. Barone, B. Mennucci and G. Petersson, *Inc., Wallingford CT*, 2009, **201**.

12. H. Ma, S. Chen, Z. Liu and Y. Sun, *Journal of Molecular Structure: THEOCHEM*, 2006, **774**, 19-22.

13. C. Lee, W. Yang and R. G. Parr, *Physical review B*, 1988, **37**, 785.

14. A. D. Becke, *The Journal of chemical physics*, 1992, **96**, 2155-2160.

15. S. H. Vosko, L. Wilk and M. Nusair, *Canadian Journal of physics*, 1980, **58**, 1200-1211.

16. M. Xu, Y. Liu, B. Li, W. Li, X. Li and S. Hu, *Electrochemistry communications*, 2012, **18**, 123-126.

17. L. Xing, W. Li, M. Xu, T. Li and L. Zhou, *Journal of Power Sources*, 2011, **196**, 7044-7047.

18. L. Xing, X. Zheng, M. Schroeder, J. Alvarado, A. von Wald Cresce, K. Xu, Q. Li and W. Li, *Accounts of chemical research*, 2018, **51**, 282-289.

19. S. Junaedi, A. A. Al-Amiery, A. Kadihum, A. A. H. Kadhum and A. B. Mohamad, *International Journal of Molecular Sciences*, 2013, **14**.

20. T. Arslan, F. Kandemirli, E. E. Ebenso, I. Love and H. Alemu, *Corrosion Science*, 2009, **51**, 35-47.

21. A. Zarrouk, B. Hammouti, A. Dafali, M. Bouachrine, H. Zarrok, S. Boukhris and S. S.

Al-Deyab, *Journal of Saudi Chemical Society*, 2014, **18**, 450-455.

22. H. Ju, Z.-P. Kai and Y. Li, *Corrosion Science*, 2008, **50**, 865-871.

23. T. M. Tekaligne, S. K. Merso, S.-C. Yang, S.-C. Liao, F.-Y. Tsai, F. W. Fenta, H. K. Bezabih, K. N. Shitaw, S.-K. Jiang, C.-H. Wang, S.-H. Wu, W.-N. Su and B. J. Hwang, *Journal of Power Sources*, 2022, **550**, 232142.

24. S. A. Bradford, in *Corrosion Control*, ed. S. A. Bradford, Springer US, Boston, MA, 1993, DOI: 10.1007/978-1-4684-8845-6_3, pp. 33-46.

25. L. Chen, E. F. Daniel, C. Wang, C. Liu, C. Li, C. Ma, L. Wu, G. Bian, S. Chen, R. Ma, J. Dong and Y. Chen, *Electrochimica Acta*, 2023, **462**, 142744.

26. R. Fuchs-Godec and M. G. Pavlović, *Corrosion Science*, 2012, **58**, 192-201.

27. I. Mohammadi and A. Afshar, *Surface and Coatings Technology*, 2015, **278**, 48-55.

28. I. Mohammadi, A. Afshar and S. Ahmadi, *Ceramics International*, 2016, **42**, 12105-12114.

29. A. Sakuda, A. Hayashi and M. Tatsumisago, *Journal of Power Sources*, 2010, **195**, 599-603.

30. S. Ghareba and S. Omanovic, *Electrochimica Acta*, 2011, **56**, 3890-3898.

31. J. Shu, M. Shui, F. Huang, D. Xu, Y. Ren, L. Hou, J. Cui and J. Xu, *Electrochimica Acta*, 2011, **56**, 3006-3014.